ACS APPLIED NANO MATERIALS

www.acsanm.org Article

Microgels as Soluble Scaffolds for the Preparation of Noble Metal Nanoparticles Supported on Nanostructured Metal Oxides

Roberto Vescovo, Maximilian Becker, Marta Maria Natile, Patrizia Canton, Claudio Evangelisti, and Andrea Biffis*

Cite This: *ACS Appl. Nano Mater.* 2021, 4, 8343−8351 Read Online

ACCESS | Metrics & More | Article Recommendations | Supporting Information

ABSTRACT: An approach for the preparation of noble metal nanoparticles supported on nanostructured metal oxides is described herein. The approach is based on the sequential generation of the noble metal nanoparticles and of a metal oxide phase inside a cross-linked polymer colloid (microgel). By tuning the properties of the employed microgel, the nature and amount of both the noble metal nanoparticles and the metal oxide phase can be independently varied. The resulting composite colloids are colloidally stable and, upon isolation by precipitation and subsequent calcination, produce noble metal nanoparticles dispersed on a crystalline, nanostructured oxide phase. Preliminary catalytic tests provide information on the accessibility of the noble metal nanoparticles and, particularly in the case of gold, result in promising catalytic performances in the aerobic oxidation of alcohols.

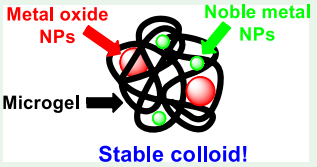

KEYWORDS: *microgel, metal oxide, nanocomposite, gold, palladium, alcohol oxidation*

INTRODUCTION

Hybrid materials consisting of intermixed inorganic and organic polymeric phases have raised considerable interest in the community of chemists and materials scientists in the course of the last decades.[1−4] The reasons for this interest are multiple and range from the development of artificial models for composite biomaterials to the use of one component as a sacrificial scaffold/template for nanostructuring the morphology of the second component (e.g., its porosity) and finally to the development of advanced composite materials, combining the properties of both components (e.g., elasticity, toughness, stimuli responsiveness, optical properties, magnetism, and catalytic activity, to name but a few);[1,2] furthermore, it is known that when such composite materials feature a high, sometimes even an ordered interface area between the two components, thanks to a high degree of mutual dispersion and/or to the nanostructuring of at least one of the phases, this may impart new properties to the composite, which are not possessed by either component taken alone.[1−12]

In recent years, synthetic approaches to these composite materials have been downscaled to the preparation of hybrid colloidal particles, with the diameter in the micron or even submicron range, which entail considerable advantages in terms of, for example, accessibility of the particles' interior, processability to form films or fibers, and readiness in the response to external stimuli. In this regard, soluble cross-linked polymer colloids (micro- or nanogels) have been increasingly employed as organic components, given their ease of preparation, variable nature and degree of functionality, colloidal stability, robustness, and fast response to stimuli.[13−18] As inorganic components, noble metals, quantum dots, inorganic oxides, metal fluorides, and other compounds have been considered, and the synthetic approaches to these composite colloids as well as their properties and potential applications have been reviewed.[19−24]

We have a long-standing experience in the chemistry of functional micro- and nanogels, in particular, on their use as soluble scaffolds for the production of hybrid colloids containing noble metal nanoparticles (NPs) to be used as quasi-homogeneous catalysts.[24−32] Together with other groups, we have pioneered the preparation of these colloids by exploiting the functional groups contained in the microgel to anchor simple metal salts or complexes as precursors, which are subsequently reduced to produce metal NPs within the microgel; in particular, our group was the first to demonstrate that using this strategy it was possible to tailor the final average size of the metal nanoparticles by acting on the morphology of the microgel scaffold through the cross-linking degree.[26] In principle, a similar strategy can also be employed for generating other kinds of inorganic components, possibly with the same degree of control on the morphology of the inorganic phase. However, despite the fact that this possibility was recognized quite early, the examples of application of this strategy to the production of hybrid colloids containing an inorganic component different from noble metals have remained quite limited. In particular, whereas some examples exist in the generation of metal chalcogenide NPs (quantum

Received: June 11, 2021
Accepted: July 29, 2021
Published: August 10, 2021

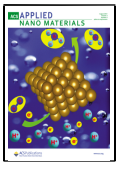

https://doi.org/10.1021/acsanm.1c01459
ACS Appl. Nano Mater. 2021, 4, 8343−8351

Table 1. Monomer Composition (% by Weight) and Hydrodynamic Radius of the Microgels Employed in this Work

microgel	MMA (% w/w)	EDMA (% w/w)	MAA (% w/w)	VP (% w/w)	hydrodynamic diameter (Z-average, nm)	PDI
MG1	40	10	50		67 (DMF)	0.50
MG2	65	10	25		40 (DMF)	0.42
MG3	40	10		50	20 (EtOH)	0.32

Scheme 1. Employed Monomers and Polymerization Procedure for the Preparation of Microgels

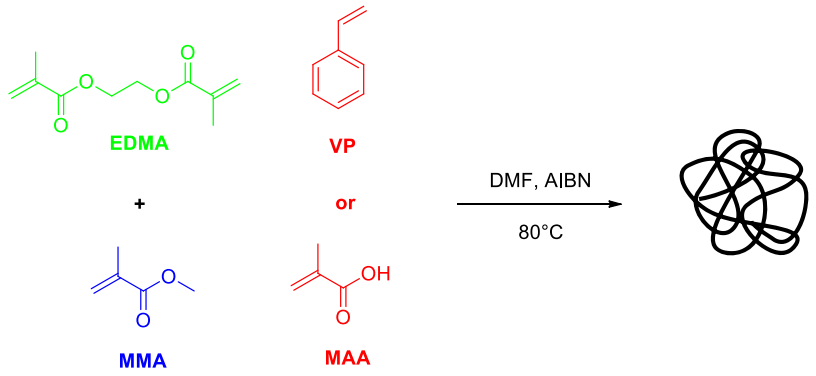

Scheme 2. Strategy for the Generation of Metal Oxide and Noble Metal Nanoparticles into Microgel Scaffolds. M = Metal Cation in Metal Oxide; M′ = Noble Metal

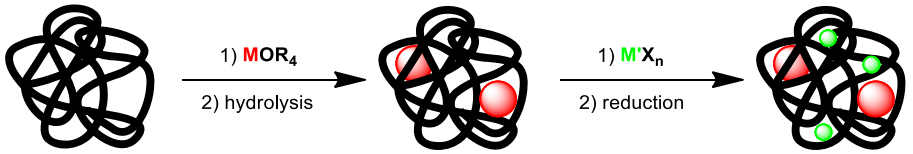

dots) within microgels,[33−35] the possibility to generate inorganic oxides has been largely overlooked, apart from studies concerning iron oxides,[36−39] silica,[40−44] or zinc oxide[45,46] as the inorganic component. With this work, we contribute to fill this gap by investigating the generation of metal oxides within microgels, with the aim of using them as nanostructured supports for metal NPs cogenerated within the same microgel.

RESULTS AND DISCUSSION

We chose to employ microgels featuring two kinds of functional groups in order to anchor metal precursors: carboxylic acid groups and pyridyl moieties. The two groups have been introduced in the microgels by using the corresponding functional comonomers, namely methacrylic acid and 4-vinylpyridine. Methyl methacrylate was employed as a nonfunctional comonomer and ethylene dimethacrylate as a cross-linker (Table 1). The microgels were synthesized by our well-established radical polymerization in dilute solution,[24,32] using *N*,*N*-dimethylformamide (DMF) as the solvent (Scheme 1), and conveniently isolated by precipitation in diethyl ether.

The next step in the synthesis of the composite materials (Scheme 2, first reaction) was the anchoring of the metal oxide precursor within the microgel and its hydrolysis with the production of the metal oxide itself. In the literature, hydrolysis is accomplished through a slow and controlled addition of water to the colloidal solution,[47,48] which in our case is practiced by simply exposing the solution to water vapor under stirring for several hours. Different ratios of metal alkoxide to microgel were used for this purpose, which we calculated in order to obtain a final weight fraction of metal oxide after hydrolysis from 0.1 (weight ratio of microgel to metal oxide, 9:1) up to 0.5 (weight ratio of microgel to metal oxide, 1:1), as we wanted to explore the extent to which we could anchor metal precursors to the microgels and subsequently form a metal oxide phase without compromising the colloidal stability of the microgel. In order to reach the highest weight fractions mentioned above, the metal oxide precursors had to be employed in molar amounts exceeding the molar amount of functional groups present in the microgel. Nevertheless, this can still result in the complete incorporation of the metal oxide phase within the microgel network, as previously reported in the literature for comparable systems;[48] in these cases, condensation to produce the metal oxide phase takes place preferentially within the microgels, in which there is a high local concentration of precursors, and successively incorporates all the metal oxide precursors present in solution.

We soon realized that the colloidal stability of the system was strongly dependent on the nature of the metal alkoxide and of the microgel. For example, microgels such as MG1 and MG2, bearing carboxylic acid groups, provided colloidally stable solutions when reacted with $Ti(OnBu)_4$ with subsequent hydrolysis, whereas the reaction with $Zr(OnBu)_4$ (in an amount corresponding to 0.33 to 0.5 weight fraction of oxide in the microgel) led to the formation of a significant amount of precipitate (probably the inorganic oxide alone) after overnight exposure to moist air. Conversely, microgel MG3 bearing pyridyl moieties as functional groups exhibited high colloidal stability when treated with $Zr(OnBu)_4$, whereas partial phase separation of a gel from the colloidal solution occurred with $Ti(OnBu)_4$ (in an amount corresponding to 0.33 to 0.5 weight fraction of oxide in the microgel) after overnight exposure to moist air. The amount of functional groups also had its importance: for example, microgel MG1 yielded less

https://doi.org/10.1021/acsanm.1c01459
ACS Appl. Nano Mater. 2021, 4, 8343−8351

satisfactory results compared to microgel MG2, which has the same chemical structure but a lower amount of pendant carboxylic acid groups; in particular, microgel MG1 started to precipitate when reacted with an amount of $Ti(OnBu)_4$ corresponding to the 0.17 weight fraction of TiO_2, whereas with microgel MG2, reaction producing up to 0.5 weight fraction of metal oxide was possible without precipitation. This difference can be explained in terms of the lower steric stabilization acting on microgel MG1 in solution, as despite the same nominal cross-linker content, a higher cross-linking is expected in MG1 due to the hydrogen bonding between the carboxylic acid groups.

The hydrolysis reactions were quantitative overnight, as could be determined by isolating the microgels loaded with metal oxide by precipitation with petroleum ether and then subjecting the product to elemental analysis: the percentage of carbon and hydrogen matched the expected values following quantitative hydrolysis, that is, they corresponded to the complete removal of the alkoxide groups of the metal oxide precursor and to the presence of the microgel scaffold as the sole organic component in the composite. Preliminary dynamic light scattering (DLS) characterization of the microgels loaded with the highest metal oxide content (0.5 weight fraction) in the same mixed solvent system in which they were prepared (moist DMF/EtOH, 1.25/1) showed, however, hydrodynamic radii between 100 and 200 nm, around 5 times larger than those of the original microgels (20−67 nm, Table 1); although somewhat larger values than in the case of pure microgels were expected after the incorporation of such a large amount of metal oxide, and allowing also for discrepancies due to the employed mixed solvent system, these differences are notable and may reflect a certain degree of aggregation of the composite microgel particles following the incorporation of the metal oxide precursors and hydrolysis. Indeed, the long-term colloidal stability of the composite microgels after hydrolysis was found to be dependent on the amount of metal oxide present: at 0.5 weight fraction of metal oxide, the resulting colloidal dispersions were stable for a few days; at 0.33, the colloids were stable over several weeks; and at 0.1, no sign of phase separation was discernible even after several months.

The structure of the inorganic phase produced after hydrolysis was briefly investigated by the X-ray diffraction (XRD) analysis of the isolated colloids in the solid state. Irrespective of the oxides employed, the inorganic phase invariably proved amorphous, and no reflections corresponding to any crystalline phase were obtained (see below). This was actually expected, as the metal oxide phase was produced by slow hydrolysis at room temperature, and under these conditions, the oxides employed in the present work do not generally form a crystalline phase.

In order to remove the microgel scaffold and to promote the crystallization of the inorganic phase, the samples were calcined at 500 °C (Scheme 3). Thermogravimetric analysis (TGA)/differential scanning calorimetry (DSC) analyses of some composite materials were preliminarily carried out in order to evaluate the temperature necessary for the decomposition reaction as well as the extent of microgel decomposition. Tests were run both in air and under dinitrogen as an inert gas. The tests revealed that the decomposition of both microgels MG2 and MG3 took place below 500 °C and that the removal of the organic component was essentially complete in air (Figure S1), whereas some

Scheme 3. Generation of Crystalline Inorganic Nanocomposites from Microgels Containing Amorphous Inorganic Oxide NPs (Red) and Noble Metal NPs (Green)

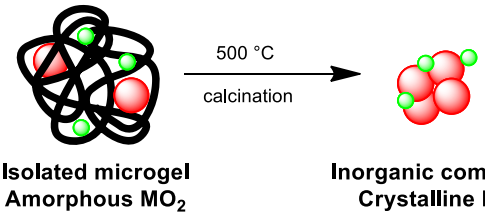

carbonaceous residue remained in the composite materials when heating was performed in an inert atmosphere. Consequently, all calcination processes were run at 500 °C under air.

The inorganic residue produced upon calcination was again subjected to XRD analysis, which confirmed this time, as expected, the crystallinity of the metal oxide sample. As it will be discussed in more detail below, in the context of the preparation of the composites, microgels loaded with titanium dioxide produced mainly anatase as the crystalline phase, whereas pure tetragonal zirconia was produced by these means in the case of zirconium dioxide; finally, in the case of cerium dioxide, cerianite was produced.

Having established the possibility to produce crystalline inorganic oxide samples by this mean, we then investigated on the production of ternary microgels featuring both an inorganic oxide phase and noble metal NPs. As mentioned in Introduction, noble metal NPs can be conveniently generated inside microgels by anchoring suitable metal precursors, followed by chemical reduction (Scheme 2, second reaction).[24−32] In principle, the generation of the noble metal NPs can precede or follow the anchoring of the metal oxide precursors and the consequent formation of the metal oxide phase within the microgel by hydrolysis. The preference for either approach depends on the need for the intermediate isolation of the hybrid microgel containing the noble metal NPs. If the microgel solution resulting from the reduction of the noble metal precursors can be directly employed for the production of the metal oxide phase, then this reaction sequence can be conveniently followed. Otherwise, it is more practical to produce the metal oxide first and produce the noble metal NPs afterward, isolating the composite colloids from the reaction mixture only in the last step. In the latter case, one can also choose to produce the noble metal NPs before or after the hydrolysis step of the metal oxide precursors; the choice essentially depends on the nature of the noble metal and particularly of the reducing agent employed for NP synthesis. Thus, with Pd as the noble metal, all possible approaches are equally practical; hence, the microgels were charged with a solution of palladium(II) nitrate and subsequently reduced either before or after the generation of the metal oxide phase. The reduction of palladium(II) took place very easily, as the ethanol cosolvent is already a sufficiently strong reducing agent and gentle heating of the microgel solution to reflux produced the corresponding Pd NPs. On the other hand, in the case of Au, contrary to previous reports on closely related systems,[49] the reduction procedure using the ethanol cosolvent as the reducing agent was found to be slow and ineffective, leading to incomplete gold reduction, as shown also by the X-ray photoelectron spectroscopy (XPS) analysis of the final material (see below). A stronger reducing

https://doi.org/10.1021/acsanm.1c01459
ACS Appl. Nano Mater. 2021, 4, 8343−8351

agent, such as excess sodium triethylborohydride, was necessary, which due to its sensitivity to water could not be employed after the hydrolysis step. Consequently, in this case, the microgels were first loaded with the metal oxide precursor and then with gold(III) chloride hydrate, which was subsequently reduced to Au NPs before the actual hydrolysis of the metal oxide precursors. The resulting ternary composite microgels produced with these approaches are listed in Table 2.

Table 2. Ternary Composite Microgels Prepared in the Frame of this Work

sample	microgel	metal oxide[a] (wt. fraction)	noble metal[b]	method	reducing agent
MG2TiPd5a	MG2	TiO_2 (0.5)	Pd	oxide first	EtOH
MG2TiPd3.3a	MG2	TiO_2 (0.33)	Pd	oxide first	EtOH
MG2TiPd5b	MG2	TiO_2 (0.5)	Pd	NP first	EtOH
MG3TiPd5a[c]	MG3	TiO_2 (0.5)	Pd	oxide first	EtOH
MG2TiPd3.3b	MG2	TiO_2 (0.33)	Pd	NP first	EtOH
MG2ZrPd5a[d]	MG2	ZrO_2 (0.5)	Pd	oxide first	EtOH
MG3ZrPd5a	MG3	ZrO_2 (0.5)	Pd	oxide first	EtOH
MG3ZrPd3.3a	MG3	ZrO_2 (0.33)	Pd	oxide first	EtOH
MG3ZrAu5c	MG3	ZrO_2 (0.5)	Au	oxide first	$NaBHEt_3$
MG3ZrAu3.3a	MG3	ZrO_2 (0.33)	Au	oxide first	EtOH
MG3ZrAu3.3c	MG3	ZrO_2 (0.33)	Au	oxide first	$NaBHEt_3$
MG3CeAu3.3a	MG3	CeO_2 (0.33)	Au	oxide first	EtOH
MG3CeAu3.3c	MG3	CeO_2 (0.33)	Au	oxide first	$NaBHEt_3$

[a]Weight fraction of the metal oxide in the uncalcined composite. [b]Noble metal content is 0.1 equiv. with respect to the metal oxide in all cases. [c]A gel was partially formed during the synthesis (see text). [d]A trace of precipitate was formed during the synthesis (see text).

Composite microgel samples were characterized by XRD analyses before calcination, which highlighted, as expected, the presence of crystalline noble metal NPs within the microgels and the amorphous nature of the metal oxide contained in it. The analyses were repeated after calcination and confirmed the crystallization of the inorganic oxide and the persistence of a crystalline noble metal component within the composite material. Figure 1 reports the comparison of the XRD characterization of the products in the various stages of the preparation process.

The XRD pattern of the microgel MG2 containing 10% w/w Pd NPs shows the reflexes characteristic of cubic Pd metal NPs. Several crystalline phases are present in the patterns of the MG2TiPd5b sample and the analogous MG3TiPd5a prepared using microgel MG3 and the "oxide first" route after calcination at 500 °C. Anatase is the main phase for TiO_2, but traces of rutile are also detected. The presence of contributions pertaining to PdO indicates the oxidation of the metal Pd during the calcination process. Though the MG3TiPd5a composite colloid actually formed a gel before calcination (see above), the result of the calcination itself is useful to remark that the different nature of the organic component

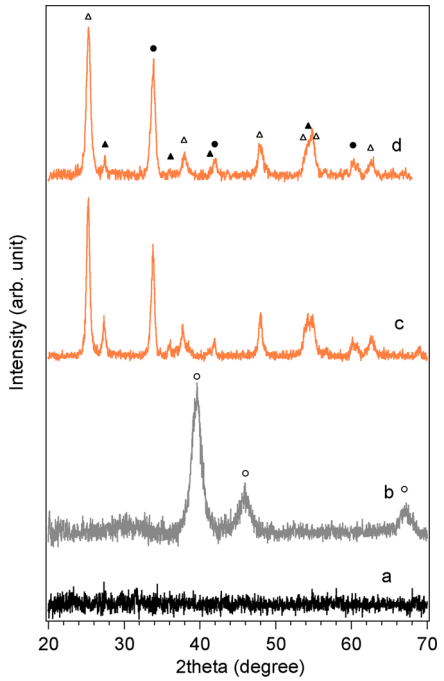

Figure 1. XRD patterns of (a) MG2 + TiO_2; (b) MG2 + 10% Pd NPs; (c) sample MG2TiPd5b after calcination; (d) sample MG3TiPd5a after calcination; △ = TiO_2 anatase (JCPDS card#00-021-1272); ▲ = TiO_2 rutile (JCPDS card#00-021-1276); ◯ = Pd (JCPDS card#01-087-0641); ● = PdO (JCPDS card#00-041-1107). For comparison purpose, the patterns are normalized with respect to their maximum and minimum.

provides no significant difference in the final result of the calcination process. The crystallite sizes, estimated by the Scherrer equation, resulted 18 and 13 nm for anatase in MG2TiPd5b and MG3TiPd5a, respectively, whereas PdO crystallite sizes resulted 19 and 15 nm for MG2TiPd5b and MG3TiPd5a, respectively. Finally, the Pd NP size in the microgel MG2 before metal oxide loading and calcination at 500 °C was estimated at 9 nm. The comparison of this datum with the PdO crystallite size in sample MG2TiPd5b derived therefrom indicates that calcination causes significant sintering of the Pd/PdO NPs. As the size of palladium-containing NPs is not expected to grow very significantly upon the oxidation of Pd to PdO,[50] we can conclude that the calcination process, apart from causing the oxidation of the Pd NPs to PdO NPs, also causes coalescence of the NPs with the production of larger particles and aggregates.

In Figure 2 the XRD patterns of composite materials containing zirconia and ceria are shown instead. It can be appreciated that tetragonal zirconia is always obtained, irrespective of the nature of the employed microgel and of the noble metal NPs contained in the material before calcination. This is a very interesting result considering that tetragonal ZrO_2 is stable between 1200 and 2300 °C, and few procedures allow to obtain it at a lower temperature. Furthermore, CeO_2 with the fluorite structure (cerianite) is obtained in the case of ceria. With regard to the noble metal NPs, oxidation of Pd to PdO also occurs in this case, whereas gold NPs are expectedly (given the low thermal stability of the oxide) not oxidized during the calcination process.

The average size of the PdO NPs produced after calcination was found to be in the range 10−15 nm in all cases, whereas larger NPs (15−40 nm) were obtained in the case of gold, the

https://doi.org/10.1021/acsanm.1c01459
ACS Appl. Nano Mater. 2021, 4, 8343−8351

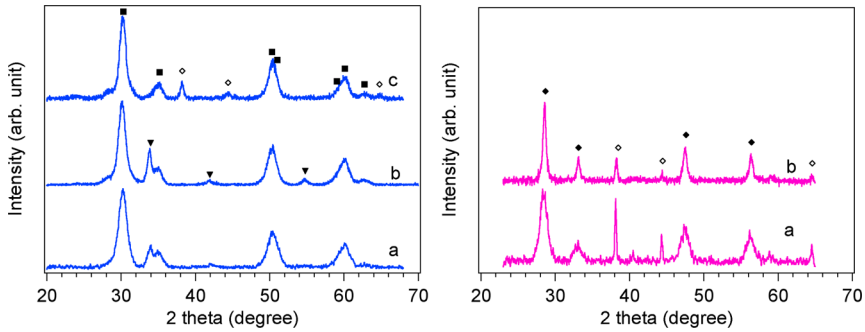

Figure 2. XRD patterns of (A) ZrO_2-based composite materials after calcination (blue line): (a) MG3ZrPd5a; (b) MG2ZrPd5a; and (c) MG3ZrAu3.3a. (B) CeO_2-based composite materials (magenta line) after calcination: (a) MG3CeAu3.3a and (b) MG3CeAu3.3c. ■ = ZrO_2 tetragonal (JCPDS card#00-050-1089); ● = PdO (JCPDS card#00-041-1107); ◆ = CeO_2 cubic (JCPDS card#01-078-0694); ◇ = Au cubic (JCPDS card#00-004-0784). For comparison purpose, the patterns are normalized with respect to their maximum and minimum.

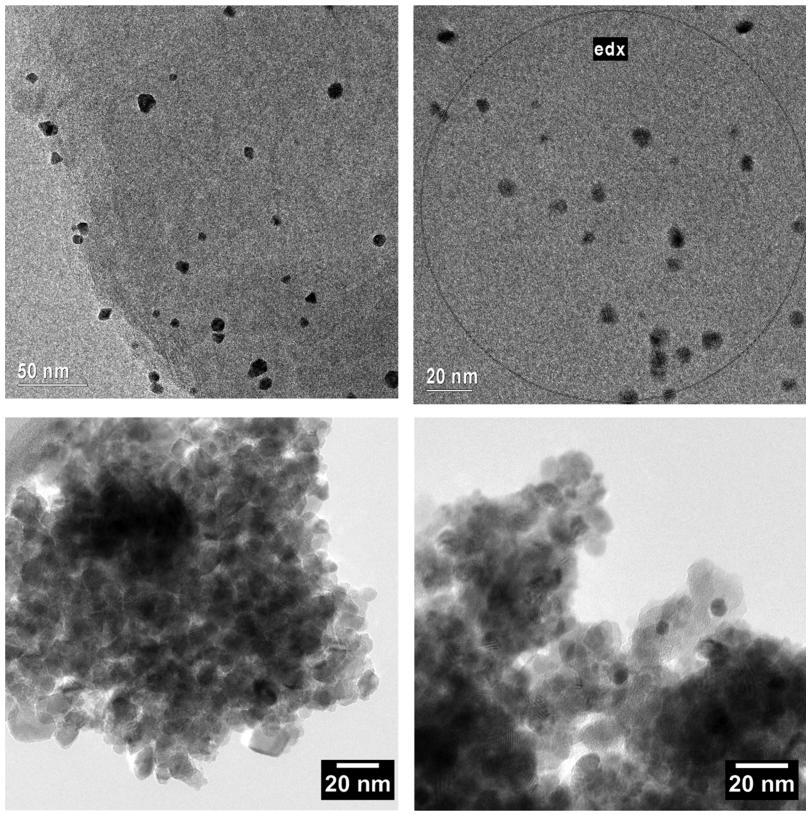

Figure 3. TEM micrographs of MG2 + 5% Pd NPs (top left), of composite MG2TiPd3.3a before calcination (top right), and of composite materials obtained upon calcination: MG2TiPd3.3a (bottom left) and MG3ZrAu3.3c (bottom right).

largest sizes being reached as expected using EtOH as the reducing agent (a slow reducing agent causes a slow nucleation rate and consequently the growth of larger NPs).

Transmission electron microscopy (TEM) analysis of the samples (see, e.g., Figure 3) confirmed the data obtained from XRD and also pointed out that the noble metal/metal oxide NPs after calcination exhibited a rather broad size distribution and significant aggregation. It needs to be recalled that results previously obtained in the generation of Pd or Au NPs inside microgels[24−32] generally indicate the production of more monodisperse NPs in the range 3−5 nm. Indeed, the determination of the average size and size distribution of Pd NPs inside microgel MG2 (Figure S2) as well as inside composites before calcination confirmed that the NPs before calcination are much more monodisperse and in the size range 5−10 nm, irrespective of their generation before (Figure 3, top left) or after (Figure 3, top right) the formation of the metal oxide inside the microgel. The larger sizes of the noble metal NPs recorded in these preparations compared to previous ones depend on the unoptimized reaction conditions and on the employed higher concentrations of noble metals (5−10 wt.%).

The TEM micrograph of the sample MG2TiPd3.3a before calcination (Figure 3, top right) also shows no discernible features from the presence of the amorphous TiO_2 phase, which is however easily detectable upon the energy-dispersive X-ray spectroscopy (EDX) analysis of the sample (Figure S3). On the other hand, TEM micrographs after calcination (Figure 3, bottom left) show well the crystalline TiO_2 phase as agglomerates of nanoparticles in the 10−15 nm size range, as also determined by XRD (see above).

https://doi.org/10.1021/acsanm.1c01459
ACS Appl. Nano Mater. 2021, 4, 8343−8351

Scheme 4. Suzuki Coupling Reaction Investigated in the Present Work

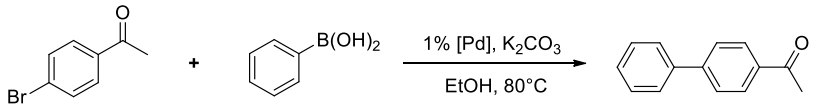

Summarizing, TEM and XRD analyses support the conclusion that the calcination process, apart from promoting crystallization of the metal oxide phase and oxidation of the Pd NPs to PdO NPs, also causes coalescence of the NPs with the production of larger particles and aggregates, and that this process is significantly more pronounced in the case of gold. Indeed, recent reports on the temperature stability of Au NPs pointed out that the onset of coalescence phenomena is at around 300 °C.[51] We are currently investigating on the possibility to obtain the removal of the organic component and/or the crystallization of the inorganic oxide component at lower temperatures in order to avoid extensive restructuring of the noble metal component in the composite.

The information provided by XRD, particularly regarding the oxidation state of the noble metal NPs, was confirmed by XPS analyses of the samples. With regard to the composite samples containing Au NPs, XPS analysis revealed significant differences, depending on the reducing agent used. Whereas samples reduced with sodium triethylborohydride exhibited only signals associated with gold(0), this was not the case for the sample reduced with ethanol, in which apparently a fraction of unreduced gold(III) remained in the sample even after calcination. The peak shape and bending energies (BEs) (84.0 and 87.7 eV for Au $4f_{7/2}$ and $4f_{5/2}$, respectively) measured for the Au 4f peak in MG3ZrAu3.3c are fully coherent with the exclusive presence of Au(0).[52] Moving to the MG3ZrAu3.3a sample, the fitting procedure reveals the presence of two Au 4f doublets: beside the one ascribable to Au(0), another one at higher BEs (88.4 and 92.1 eV) suggests the presence of a minor quantity of Au(III) on the sample surface (Figure S4).[53] The percentages of Au(0) and Au(III) in the sample MG3ZrAu3.3a are 72 and 28%, respectively. Concerning the samples containing Pd (Figure S4), the BEs measured for Pd $3d_{5/2}$ and $3d_{3/2}$ (336.6 and 341.8 eV, respectively) of the sample MG2TiPd5a after calcination are in agreement with the values reported in the literature for Pd(II) in PdO.[54]

As the prereduction of Pd to the zerovalent state is often a requirement for the application of heterogeneous Pd catalysts, we set out to investigate on the ease with which the PdO NPs produced within the nanocomposites after calcination were reduced to Pd metal. Temperature-programmed reduction (TPR) experiments with dihydrogen were run in order to assess this point. The experiments provided some contrasting results. The analysis of calcined samples supported on zirconia evidenced indeed a reduction peak for Pd at a temperature of 60 °C (se e.g. Figure S5), which is in line with the observations reported in the literature.[55] On the other hand, calcined samples supported on titania did not show a reduction peak at all, which apparently supports the fact that PdO NPs are in this case embedded within the titania matrix and not accessible even to gaseous reactants such as dihydrogen. However, both XPS and XRD analyses of the calcined sample MG2TiPd5a after TPR provided evidence of at least a partial reduction of PdO to Pd in this sample (Figures S3 and S5). It is to point out, though, that the TPR treatment, with heating up to 900 °C, produces a significant change in the TiO_2 and ZrO_2 structures. After TPR, TiO_2 is present as rutile, while two different phases of ZrO_2 are evident in the XRD pattern: beside tetragonal ZrO_2, a monoclinic phase is also formed (Figure S6). We can conclude that even in the case of titania the PdO NPs are reducible but that the reduction process is much more sluggish and difficult than in the case of zirconia. As the starting average NP sizes are comparable in the two materials, the different ease of reduction may depend on the different locations of the NPs in the metal oxide matrix in the two cases, the PdO NPs being more exposed on zirconia than on titania. Structural changes in the crystalline metal oxide phase taking place at high temperatures (>500 °C) might modify the accessibility of the PdO NPs and facilitate their reduction.

Finally, the morphology of the calcined samples was investigated by scanning electron microscopy (SEM). The metal oxide support, irrespective of its nature, almost invariably exhibited a rather compact morphology, with very little indication of the presence of porosity (Figure S7). Only in the case of titania, some structuration in the form of coagulated spherical nodules of tens of nanometers size was apparent (Figure S7, above). Variations in the nature of the microgel (MG2 or MG3) and in the weight fraction of the metal oxide before calcination (0.5 or 0.33) also had no significant consequence on the morphology. Thus, we can conclude that the microgel structure is not rigid enough to template the generation of a pore system inside the oxide upon calcination. We suppose that this inability has a lot to do with the amorphous nature of the metal oxide that is produced upon hydrolysis; consequently, ongoing research is currently targeted toward the development of synthetic strategies that allow the production of crystalline metal oxides inside microgels under conditions at which the microgel is thermally stable and possibly also colloidally stable.

Noble metal/metal oxide nanocomposites can display peculiar and interesting catalytic properties.[56] A preliminary screening of the catalytic performance of the calcined materials was therefore carried out on two separate target reactions for palladium and gold-based samples. Palladium-containing samples were employed as precatalysts in a standard cross-coupling reaction, such as the Suzuki reaction of 4-bromoacetophenone with phenylboronic acid (Scheme 4).

The Suzuki reaction has become one of the most widely employed standard reactions to evaluate the reactivity of palladium-containing soluble species as well as heterogeneous Pd metal-[57] or PdO-containing precatalysts.[58] These heterogeneous systems generally operate upon releasing into the solution homogeneous, catalytically competent species[56] and reach in some cases remarkable catalytic activities.[57−59] However, with the composite system containing PdO prepared in this study, the catalytic activity was very low. Several catalysts showed no conversion at all under the reaction conditions reported in Scheme 4, and only with some PdO/ZrO_2 precatalysts, it was possible to record some catalytic activity. However, even the most active catalyst, MG3ZrPd5a, only reached 37% conversion of 4-bromoacetophenone after 20 h reaction time, which is a performance far below that of

https://doi.org/10.1021/acsanm.1c01459
ACS Appl. Nano Mater. 2021, 4, 8343−8351

Scheme 5. Aerobic Alcohol Oxidation Reaction Investigated in the Present Work

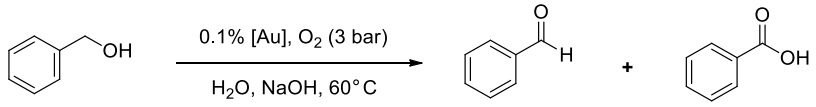

current reference catalysts based on PdO with the same standard substrates under comparable or even milder reaction conditions.[59] An explanation that can be provided for this different behavior relies on the accessibility of the PdO NPs, which in the present case are probably embedded in the metal oxide matrix and are largely unavailable for reaction.

A preliminary catalytic test on gold-containing composites targeted instead another benchmark reaction typical for gold(0),[60−62] namely the aerobic oxidation of benzyl alcohol (Scheme 5). The results are reported in Table 3.

Table 3. Results of the Catalytic Tests in the Aerobic Oxidation of Benzyl Alcohol[a]

			yield %		
test	Catalyst	average $TOF_{t=3h}$ (h^{-1})	aldehyde	acid	total
1	MG3ZrAu3.3a	28	5.5	2.8	8.3
2	MG3CeAu3.3a	0	0.0	0.0	0.0
3	MG3ZrAu5c	87	12	14	26
4	MG3ZrAu3.3c	94	11	17	28
5	MG3CeAu3.3c	138	13	28	41

[a]Reaction conditions: 0.2 M benzyl alcohol and 0.2 M NaOH in water, 0.1 mol % [Au], 3 atm O_2, 60 °C, 3 h.

In the case of this reaction, reasonable activity was recorded with the composites, which is comparable to other catalysts based on gold NPs supported on inorganic oxides, typically exhibiting TOFs in the range of tens to hundreds $hours^{-1}$ for the same reaction.[63,64] Unsurprisingly, best results were recorded with composites prepared using sodium triethylborohydride as the reducing agent for Au NP generation (Table 3, entries 3−5), which results in smaller sizes and narrower size distributions for gold particles. In this group of composite catalysts, CeO_2 emerges as the best metal oxide support (Table 3, entry 5), which is in line with the recognized privileged nature of this oxide as the support due to the potential active role that it can assume in the aerobic oxidation process.[63] Further optimization of this composite catalyst is currently underway and will involve the development of methodologies for achieving a higher degree of control on the Au NP size and size distribution[64] as well as an investigation on the possibility to photoactivate the catalyst.[65]

CONCLUSIONS

In conclusion, we have demonstrated that microgels can be employed as soluble scaffolds for the sequential cogeneration of noble metal nanoparticles and amorphous metal oxides inside the swollen microgel particles, without compromising the colloidal stability of the microgel solutions. The resulting ternary nanocomposites can be isolated and furnish nanostructured materials upon calcination with the removal of the organic component, consisting in dispersions of noble metal nanoparticles on a crystalline inorganic oxide phase. The final inorganic nanostructured material can act as the catalyst for technologically relevant chemical reactions. Work currently in progress is aimed on the one hand at the generation of crystalline metal oxide nanoparticles within microgels in solution, using in particular hydrothermal techniques, and on the other hand at achieving a higher degree of control in the generation of inorganic nanocomposite materials, in terms, for example, of the degree of metal dispersion, localization of the noble metal NPs, and morphology and porosity of the metal oxide phase. Achieving such a high degree of control will allow to optimize the present method for a large-scale, economical production of transition-metal oxides doped with noble metal nanoparticles for a plethora of applications.

ASSOCIATED CONTENT

Supporting Information

The Supporting Information is available free of charge at https://pubs.acs.org/doi/10.1021/acsanm.1c01459.

Experimental procedures and additional characterization data (TGA curves, size distribution and EDX data from TEM analysis, additional XPS and XRD spectra, TPR curve, and SEM micrographs) (PDF)

AUTHOR INFORMATION

Corresponding Author

Andrea Biffis − *Dipartimento di Scienze Chimiche, Università di Padova, Padova I-35131, Italy;* orcid.org/0000-0002-7762-8280; Phone: +39-049-827-5216; Email: andrea.biffis@unipd.it; Fax: +39-049-8275223

Authors

Roberto Vescovo − *Dipartimento di Scienze Chimiche, Università di Padova, Padova I-35131, Italy*

Maximilian Becker − *Dipartimento di Scienze Chimiche, Università di Padova, Padova I-35131, Italy*

Marta Maria Natile − *Dipartimento di Scienze Chimiche, Università di Padova, Padova I-35131, Italy; Istituto di Chimica della Materia Condensata e Tecnologie per l'Energia—ICMATE, Consiglio Nazionale delle Ricerche—CNR, Padova I-35131, Italy;* orcid.org/0000-0001-5591-2670

Patrizia Canton − *Dipartimento di Scienze Molecolari e Nanosistemi, Università Ca' Foscari Venezia, Venezia-Mestre I-30170, Italy;* orcid.org/0000-0003-1604-5265

Claudio Evangelisti − *Istituto di Scienze e Tecnologie Chimiche—SCITEC, Consiglio Nazionale delle Ricerche—CNR, Milano I-20133, Italy;* Present Address: Istituto di Chimica dei Composti Organometallici—ICCOM, Consiglio Nazionale delle Ricerche—CNR, Area della Ricerca CNR di Pisa, Via Moruzzi 1, I-56124 Pisa, Italy

Complete contact information is available at: https://pubs.acs.org/10.1021/acsanm.1c01459

Notes

The authors declare no competing financial interest.

ACKNOWLEDGMENTS

The authors would like to thank Roberta Saini, University of Padova, for the TGA measurements and Prof. Antonella

Glisenti, University of Padova, for the TPR analysis. M.B. thanks the Erasmus+ program for a scholarship. M.M.N. acknowledges the MIUR-PON TARANTO (ARS01_00637) for partial funding.

REFERENCES

(1) Mobin, R.; Rangreez, T. A.; Chisti, H. T. N.; Inamuddin; Rezakazemi, M. Organic-Inorganic Hybrid Materials and Their Applications. In *Functional Polymers*; Jafar Mazumder, M. A., Sheardown, H., Al-Ahmed, A., Eds.; Springer International Publishing: Cham, 2019; pp 1135−1156.
(2) Faustini, M.; Nicole, L.; Ruiz-Hitzky, E.; Sanchez, C. History of Organic-Inorganic Hybrid Materials: Prehistory, Art, Science, and Advanced Applications. *Adv. Funct. Mater.* **2018**, *28*, 1704158.
(3) Mir, S. H.; Nagahara, L. A.; Thundat, T.; Mokarian-Tabari, P.; Furukawa, H.; Khosla, A. Review-Organic-Inorganic Hybrid Functional Materials: An Integrated Platform for Applied Technologies. *J. Electrochem. Soc.* **2018**, *165*, B3137−B3156.
(4) Thakur, V. K.; Thakur, M. K.; Pappu, A.; Gupta, R. K. *Hybrid Polymer Composite Materials. Structure and Chemistry*; Woodhead Publishing, an imprint of Elsevier: Duxford, 2017.
(5) Zhang, D.; Yang, Z.; Yu, S.; Mi, Q.; Pan, Q. Diversiform Metal Oxide-Based Hybrid Nanostructures for Gas Sensing with Versatile Prospects. *Coord. Chem. Rev.* **2020**, *413*, 213272.
(6) Pan, Z.; Yao, L.; Zhai, J.; Yao, X.; Chen, H. Interfacial Coupling Effect in Organic/Inorganic Nanocomposites with High Energy Density. *Adv. Mater.* **2018**, *30*, 1705662.
(7) Peng, S.; Jin, G.; Li, L.; Li, K.; Srinivasan, M.; Ramakrishna, S.; Chen, J. Multi-functional electrospun nanofibres for advances in tissue regeneration, energy conversion & storage, and water treatment. *Chem. Soc. Rev.* **2016**, *45*, 1225−1241.
(8) Song, F.; Li, X.; Wang, Q.; Liao, L.; Zhang, C. Nanocomposite Hydrogels and Their Applications in Drug Delivery and Tissue Engineering. *J. Biomed. Nanotechnol.* **2015**, *11*, 40−52.
(9) Ng, L. Y.; Mohammad, A. W.; Leo, C. P.; Hilal, N. Polymeric Membranes Incorporated with Metal/Metal Oxide Nanoparticles: A Comprehensive Review. *Desalination* **2013**, *308*, 15−33.
(10) Kao, J.; Thorkelsson, K.; Bai, P.; Rancatore, B. J.; Xu, T. Toward Functional Nanocomposites: Taking the Best of Nanoparticles, Polymers, and Small Molecules. *Chem. Soc. Rev.* **2013**, *42*, 2654−2678.
(11) Thakur, V. K.; Ding, G.; Ma, J.; Lee, P. S.; Lu, X. Hybrid Materials and Polymer Electrolytes for Electrochromic Device Applications. *Adv. Mater.* **2012**, *24*, 4071−4096.
(12) Jancar, J.; Douglas, J. F.; Starr, F. W.; Kumar, S. K.; Cassagnau, P.; Lesser, A. J.; Sternstein, S. S.; Buehler, M. J. Current issues in research on structure-property relationships in polymer nanocomposites. *Polymer* **2010**, *51*, 3321−3343.
(13) Plamper, F. A.; Richtering, W. Functional Microgels and Microgel Systems. *Acc. Chem. Res.* **2017**, *50*, 131−140.
(14) Hamzah, Y. B.; Hashim, S.; Rahman, W. A. W. A. Synthesis of Polymeric Nano/Microgels: A Review. *J. Polym. Res.* **2017**, *24*, 134.
(15) *Microgel Suspensions: Fundamentals and Applications*; Fernandez-Nieves, A., Ed.; Wiley-VCH: Weinheim, Germany, 2011.
(16) *Chemical Design of Responsive Microgels*; Pich, A., Richtering, W., Eds.; Advances in Polymer Science; Springer: Berlin, Heidelberg, 2011; Vol. *234*.
(17) Thorne, J. B.; Vine, G. J.; Snowden, M. J. Microgel Applications and Commercial Considerations. *Colloid Polym. Sci.* **2011**, *289*, 625−646.
(18) Fernández-Barbero, A.; Suárez, I. J.; Sierra-Martín, B.; Fernández-Nieves, A.; de las Nieves, F. J.; Marquez, M.; Rubio-Retama, J.; López-Cabarcos, E. Gels and Microgels for Nanotechnological Applications. *Adv. Colloid Interface Sci.* **2009**, *147-148*, 88−108.
(19) Centomo, P.; Zecca, M.; Biffis, A. Cross-Linked Polymers as Scaffolds for the Low-Temperature Preparation of Nanostructured Metal Oxides. *Chem.—Eur. J.* **2020**, *26*, 9243−9260.
(20) Echeverria, C.; Fernandes, S.; Godinho, M.; Borges, J.; Soares, P. Functional Stimuli-Responsive Gels: Hydrogels and Microgels. *Gels* **2018**, *4*, 54.
(21) Sierra-Martin, B.; Fernandez-Barbero, A. Inorganic/Polymer Hybrid Nanoparticles for Sensing Applications. *Adv. Colloid Interface Sci.* **2016**, *233*, 25−37.
(22) Pérez-Juste, J.; Pastoriza-Santos, I.; Liz-Marzán, L. M. Multifunctionality in Metal@microgel Colloidal Nanocomposites. *J. Mater. Chem. A* **2013**, *1*, 20−26.
(23) Karg, M. Multifunctional Inorganic/Organic Hybrid Microgels. *Colloid Polym. Sci.* **2012**, *290*, 673−688.
(24) Biffis, A. Microgels as Exotemplates in the Synthesis of Size Controlled Metal Nanoclusters. In *Metal Nanoclusters in Catalysis and Materials Science: The Issue of Size Control*; Corain, B., Schmid, G., Toshima, N., Eds.; Elsevier: Amsterdam, 2008; pp. 341−346.
(25) Biffis, A. Functionalised Microgels: Novel Stabilisers for Catalytically Active Metal Colloids. *J. Mol. Catal. A: Chem.* **2001**, *165*, 303−307.
(26) Biffis, A.; Orlandi, N.; Corain, B. Microgel-Stabilized Metal Nanoclusters: Size Control by Microgel Nanomorphology. *Adv. Mater.* **2003**, *15*, 1551−1555.
(27) Biffis, A.; Sperotto, E. Microgel-Stabilized Metal Nanoclusters: Improved Solid-State Stability and Catalytic Activity in Suzuki Couplings. *Langmuir* **2003**, *19*, 9548−9550.
(28) Biffis, A.; Minati, L. Efficient Aerobic Oxidation of Alcohols in Water Catalysed by Microgel-Stabilised Metal Nanoclusters. *J. Catal.* **2005**, *236*, 405−409.
(29) Biffis, A.; Cunial, S.; Spontoni, P.; Prati, L. Microgel-Stabilized Gold Nanoclusters: Powerful "Quasi-Homogeneous" Catalysts for the Aerobic Oxidation of Alcohols in Water. *J. Catal.* **2007**, *251*, 1−6.
(30) Piperno, S.; Gheber, L. A.; Canton, P.; Pich, A.; Dvorakova, G.; Biffis, A. Microgel Electrospinning: A Novel Tool for the Fabrication of Nanocomposite Fibers. *Polymer* **2009**, *50*, 6193−6197.
(31) Contin, A.; Biffis, A.; Sterchele, S.; Dörmbach, K.; Schipmann, S.; Pich, A. Metal Nanoparticles inside Microgel/Clay Nanohybrids: Synthesis, Characterization and Catalytic Efficiency in Cross-Coupling Reactions. *J. Colloid Interface Sci.* **2014**, *414*, 41−45.
(32) Cera, G.; Biffis, A.; Canton, P.; Villa, A.; Prati, L. Metal Nanoclusters Stabilized by PH-Responsive Microgels: Preparation and Evaluation of Their Catalytic Potential. *React. Funct. Polym.* **2017**, *115*, 81−86.
(33) Xu, S.; Zhang, J.; Paquet, C.; Lin, Y.; Kumacheva, E. From Hybrid Microgels to Photonic Crystals. *Adv. Funct. Mater.* **2003**, *13*, 468−472.
(34) Pich, A.; Hain, J.; Lu, Y.; Boyko, V.; Prots, Y.; Adler, H.-J. Hybrid Microgels with ZnS Inclusions. *Macromolecules* **2005**, *38*, 6610−6619.
(35) Liu, J.; Shu, T.; Su, L.; Zhang, X.; Serpe, M. J. Synthesis of poly (N-isopropylacrylamide)-co-(acrylic acid) microgel-entrapped CdS quantum dots and their photocatalytic degradation of an organic dye. *RSC Adv.* **2018**, *8*, 16850−16857.
(36) Zhang, J.; Xu, S.; Kumacheva, E. Polymer Microgels: Reactors for Semiconductor, Metal, and Magnetic Nanoparticles. *J. Am. Chem. Soc.* **2004**, *126*, 7908−7914.
(37) Pich, A.; Bhattacharya, S.; Lu, Y.; Boyko, V.; Adler, H.-J. P. Temperature-Sensitive Hybrid Microgels with Magnetic Properties. *Langmuir* **2004**, *20*, 10706−10711.
(38) Bhattacharya, S.; Eckert, F.; Boyko, V.; Pich, A. Temperature-, pH-, and Magnetic-Field-Sensitive Hybrid Microgels. *Small* **2007**, *3*, 650−657.
(39) Yao, H.; Li, X.; Shi, X.; Qiu, G.; Lu, X. Synthesis and Self-Assembly of Multiple-Responsive Magnetic Nanogels. *Polym. Adv. Technol.* **2019**, *30*, 312−319.
(40) Zhou, F.; Li, S.; Vo, C. D.; Yuan, J.-J.; Chai, S.; Gao, Q.; Armes, S. P.; Lu, C.; Cheng, S. Biomimetic Deposition of Silica Templated by a Cationic Polyamine-Containing Microgel. *Langmuir* **2007**, *23*, 9737−9744.

https://doi.org/10.1021/acsanm.1c01459
ACS Appl. Nano Mater. 2021, 4, 8343−8351

(41) Agrawal, G.; Schürings, M.; Zhu, X.; Pich, A. Microgel/SiO2 Hybrid Colloids Prepared Using a Water Soluble Silica Precursor. *Polymer* **2012**, *53*, 1189−1197.
(42) Dechézelles, J.-F.; Malik, V.; Crassous, J. J.; Schurtenberger, P. Hybrid Raspberry Microgels with Tunable Thermoresponsive Behavior. *Soft Matter* **2013**, *9*, 2798−2802.
(43) Cao-Luu, N.-H.; Pham, Q.-T.; Yao, Z.-H.; Wang, F.-M.; Chern, C.-S. Synthesis and characterization of poly(N-isopropylacrylamide-co-N,N′-methylenebisacrylamide-co-acrylamide) core - Silica shell nanoparticles by using reactive surfactant polyoxyethylene alkylphenyl ether ammonium sulfate. *Eur. Polym. J.* **2019**, *120*, 109263.
(44) Agrawal, G.; Samal, S. K.; Sethi, S. K.; Manik, G.; Agrawal, R. Microgel/Silica Hybrid Colloids: Bioinspired Synthesis and Controlled Release Application. *Polymer* **2019**, *178*, 121599.
(45) Agrawal, M.; Pich, A.; Gupta, S.; Zafeiropoulos, N. E.; Rubio-Retama, J.; Simon, F.; Stamm, M. Temperature Sensitive Hybrid Microgels Loaded with ZnO Nanoparticles. *J. Mater. Chem.* **2008**, *18*, 2581−2586.
(46) Wilke, P.; Coger, V.; Nachev, M.; Schachschal, S.; Million, N.; Barcikowski, S.; Sures, B.; Reimers, K.; Vogt, P. M.; Pich, A. Biocompatible Microgel-Modified Electrospun Fibers for Zinc Ion Release. *Polymer* **2015**, *61*, 163−173.
(47) Wang, X.; Hu, D.; Yang, J. Synthesis of PAM/TiO2Composite Microspheres with Hierarchical Surface Morphologies. *Chem. Mater.* **2007**, *19*, 2610−2621.
(48) Cargnello, M.; Wieder, N. L.; Montini, T.; Gorte, R. J.; Fornasiero, P. Synthesis of Dispersible Pd@CeO2Core−Shell Nanostructures by Self-Assembly. *J. Am. Chem. Soc.* **2010**, *132*, 1402−1409.
(49) Wang, M.; Pang, X.; Zheng, D.; He, Y.; Sun, L.; Lin, C.; Lin, Z. Nonepitaxial Growth of Uniform and Precisely Size-Tunable Core/Shell Nanoparticles and Their Enhanced Plasmon-Driven Photocatalysis. *J. Mater. Chem. A* **2016**, *4*, 7190−7199.
(50) Penner, S.; Wang, D.; Jenewein, B.; Gabasch, H.; Klötzer, B.; Knop-Gericke, A.; Schlögl, R.; Hayek, K. Growth and Decomposition of Aligned and Ordered PdO Nanoparticles. *J. Chem. Phys.* **2006**, *125*, 094703.
(51) Masoud, N.; Partsch, T.; de Jong, K. P.; de Jongh, P. E. Thermal Stability of Oxide-Supported Gold Nanoparticles. *Gold Bull.* **2019**, *52*, 105−114.
(52) Yu, J.; Niedenthal, W.; Smarsly, B. M.; Natile, M. M.; Huang, Y.; Carraro, M. Au Nanoparticles Supported on Piranha Etched Halloysite Nanotubes for Highly Efficient Heterogeneous Catalysis. *Appl. Surf. Sci.* **2021**, *546*, 149100.
(53) Baron, M.; Tubaro, C.; Basato, M.; Natile, M. M.; Graiff, C. Oxidative Halogenation of Dinuclear N-Heterocyclic Dicarbene Gold(I) Complexes. *J. Organomet. Chem.* **2013**, *723*, 108−114.
(54) Moulder, J. F.; Stickle, W. F.; Sobol, P. E.; Bomben, K. D. *Handbook of X-Ray Photoelectron Spectroscopy*; Chastain, J., King, Jr, R. C., Eds.; Physical Electronics Inc.: Eden Praire, 1995.
(55) Chou, C.-W.; Chu, S.-J.; Chiang, H.-J.; Huang, C.-Y.; Lee, C.-j.; Sheen, S.-R.; Perng, T. P.; Yeh, C.-t. Temperature-Programmed Reduction Study on Calcination of Nano-Palladium. *J. Phys. Chem. B* **2001**, *105*, 9113−9117.
(56) Li, G.; Tang, Z. Noble metal nanoparticle@metal oxide core/yolk-shell nanostructures as catalysts: recent progress and perspective. *Nanoscale* **2014**, *6*, 3995−4011.
(57) Biffis, A.; Centomo, P.; Del Zotto, A.; Zecca, M. Pd Metal Catalysts for Cross-Couplings and Related Reactions in the 21st Century: A Critical Review. *Chem. Rev.* **2018**, *118*, 2249−2295.
(58) Del Zotto, A.; Zuccaccia, D. Metallic palladium, PdO, and palladium supported on metal oxides for the Suzuki-Miyaura cross-coupling reaction: a unified view of the process of formation of the catalytically active species in solution. *Catal. Sci. Technol.* **2017**, *7*, 3934−3951.
(59) Karanjit, S.; Kashihara, M.; Nakayama, A.; Shrestha, L. K.; Ariga, K.; Namba, K. Highly Active and Reusable Hydrotalcite-Supported Pd(0) Catalyst for Suzuki Coupling Reactions of Aryl Bromides and Chlorides. *Tetrahedron* **2018**, *74*, 948−954.
(60) Hui, Y.; Zhang, S.; Wang, W. Recent Progress in Catalytic Oxidative Transformations of Alcohols by Supported Gold Nanoparticles. *Adv. Synth. Catal.* **2019**, *361*, 2215−2235.
(61) Carabineiro, S. A. C. Supported Gold Nanoparticles as Catalysts for the Oxidation of Alcohols and Alkanes. *Front. Chem.* **2019**, *7*, 702.
(62) Sharma, A. S.; Kaur, H.; Shah, D. Selective Oxidation of Alcohols by Supported Gold Nanoparticles: Recent Advances. *RSC Adv.* **2016**, *6*, 28688−28727.
(63) Abad, A.; Concepción, P.; Corma, A.; García, H. A Collaborative Effect between Gold and a Support Induces the Selective Oxidation of Alcohols. *Angew. Chem., Int. Ed.* **2005**, *44*, 4066−4069.
(64) Li, T.; Liu, F.; Tang, Y.; Li, L.; Miao, S.; Su, Y.; Zhang, J.; Huang, J.; Sun, H.; Haruta, M.; Wang, A.; Qiao, B.; Li, J.; Zhang, T. Maximizing the Number of Interfacial Sites in Single-Atom Catalysts for the Highly Selective, Solvent-Free Oxidation of Primary Alcohols. *Angew. Chem., Int. Ed.* **2018**, *57*, 7795−7799.
(65) Tanaka, A.; Hashimoto, K.; Kominami, H. Preparation of Au/CeO_2 Exhibiting Strong Surface Plasmon Resonance Effective for Selective or Chemoselective Oxidation of Alcohols to Aldehydes or Ketones in Aqueous Suspensions under Irradiation by Green Light. *J. Am. Chem. Soc.* **2012**, *134*, 14526−14533.

https://doi.org/10.1021/acsanm.1c01459
ACS Appl. Nano Mater. 2021, 4, 8343−8351